

Water bag modeling of a multispecies plasma

P. Morel,^{1(a)} E. Gravier,¹ N. Besse,¹ R. Klein,¹ A. Ghizzo,¹ P. Bertrand,¹ C. Bourdelle,² and X. Garbet²

¹*Institut Jean Lamour, UMR 7198 CNRS-Université Henri Poincaré, F-54506 Vandoeuvre-lès-Nancy Cedex, France*

²*Association EURATOM-CEA, CEA/DSM/IRFM, CEA Cadarache, Saint-Paul-lez-Durance, F-13108 Cedex, France*

(Received 20 January 2011; accepted 22 February 2011; published online 24 March 2011)

We report in the present paper a new modeling method to study multiple species dynamics in magnetized plasmas. Such a method is based on the gyrowater bag modeling, which consists in using a multistep-like distribution function along the velocity direction parallel to the magnetic field. The choice of a water bag representation allows an elegant link between kinetic and fluid descriptions of a plasma. The gyrowater bag model has been recently adapted to the context of strongly magnetized plasmas. We present its extension to the case of multi ion species magnetized plasmas: each ion species being modeled via a multiwater bag distribution function. The water bag modelization will be discussed in details, under the simplification of a cylindrical geometry that is convenient for linear plasma devices. As an illustration, results obtained in the linear framework for ion temperature gradient instabilities are presented, that are shown to agree qualitatively with older works. © 2011 American Institute of Physics. [doi:10.1063/1.3565019]

I. INTRODUCTION

By definition, any plasma is a multispecies one, simply regarding a pure case with electrons and just one ion population. For the sake of simplicity, most of the studies have been achieved by focusing on a given species, assuming for example the other(s) adiabatic.

From a numerical point of view, the increase of the computational power makes possible to study the coupling between different species. The limiting factor is given by the mass ratio between the different species to take into account. Even if the mass ratio between species is not so high the coupling between species increase the numerical effort, so that any alternative is welcome to decrease the dimension of a given simulation. The water bag approach has recently been demonstrated to provide such a decrease, and has motivated the present work.

From an experimental point of view strongly magnetized plasmas always include many species due to particles eroded from experiment's wall (mainly tungsten and/or carbon), that can be carried until the plasma core. In the extensively investigated case of a fusion reactor, one has to deal with tritium and deuterium for achieving the fusion reaction, and with the helium produced. Independently of their origin, such impurities could cause a non negligible loss in confinement properties and their effects on the plasma stability remains to be fully understood.

In this paper, we describe magnetically confined plasmas, characterized by negligible collision rate and high magnetic field. The toroidal version of the water bag model being under development, we present here results obtained in cylindrical geometry. Such a geometry is especially suitable for

linear plasma devices,¹⁻⁵ that offer a simplified plasma geometry with an homogeneous axisymmetric magnetic field. Moreover, such a simplification allows to recover major features of the ion temperature gradient instability that bases our investigations in the present work.

Two kinds of theoretical descriptions can be used in plasma physics: the fluid and the kinetic ones. Despite lot of progresses have been made until recent years by the use of fluid numerical solvers for studying multispecies plasmas,^{6,7} a more accurate description of microinstabilities and anomalous transport requires the use of nonlinear gyrokinetic codes.⁸⁻¹¹ In these works, the key question is about the modification of particles and heat nonlinear fluxes due to the presence of impurities and controlled by the density and temperature radial gradients. Older works concentrated on the linear response of a multispecies plasma, especially on finding the critical density and temperature gradients destabilizing the plasma,¹² and trying to give an expression for the fluxes from quasilinear theory.^{13,14}

Despite considerable progresses during last decades, gyrokinetic solvers require a huge numerical effort, and their extension to multiple species study increases such a difficulty. One can too point the fact that the operating cost of a numerical simulation of a realistic plasma becomes comparable to the one of a real experiment. Some alternative ways to describe kinetic effects with a simplified formulation are also useful, that could allow a less requiring numerical effort. Such an effort in depicting multispecies plasma can be decreased by the use of quasilinear solvers¹⁵ or gyrofluid transport models.¹⁶ The present work present another interesting alternative, based on the water bag representation.

The gyrowater-bag equations are an exact reformulation of the Vlasov Poisson system, in the case of a special form of the distribution function: the water bag which takes the form of a multistep-like distribution function along the velocity

^{a)}Electronic mail: pmorel@ulb.ac.be. Address: Physique Statistique et Plasmas, Université Libre de Bruxelles, CP 231, Campus Plaine, Boulevard du Triomphe, 1050 Brussels, Belgium.

direction (each step representing a bag). The interest of the water bag formulation consists in the discrete summation over the bags replacing the usual continuous distribution function.^{17–21} The parallel velocity dependency and the partial derivative along this direction do no more appear in equations and are replaced with the coupling between each bag dynamics ensured by a discrete summation in the quasi neutrality equation. The Vlasov Poisson system can be reformulated as a multifluid one, with an exact adiabatic closure.^{22,23}

Based on recent papers,^{23–26} that ensure the water bag model to be an interesting approach to depict kinetic features, our present work first consists in the generalization of the water bag concept to the case of a multispecies plasma, in the framework of a cylindrical geometry (Sec. II). An interesting result is that the water bag model easily offers an analytical expression of the linear stability threshold, in place of the usual Fried–Conte plasma dispersion function (Sec. III). As illustrations, linear stability frontiers are drawn in the plane of the temperature and density gradients of main ions. We then discuss the stability dependence on the nature, the ratio and the radial density and temperature profile of impurities (Sec. IV).

II. A WATER BAG APPROACH TO MODEL IMPURITIES

In the collisionless limit, each species s of a multispecies plasma is described with a Vlasov equation acting on its guiding centers distribution function $f_s = f_s(\mathbf{R}, v_{\parallel}, t)$, with \mathbf{R} defining the guiding center position, v_{\parallel} being the velocity coordinate along the magnetic field line. We consider a cylindrical geometry, assuming a constant magnetic field B oriented along the azimuthal axis called z . We assume for simplicity that the Larmor radius $r_{Ls} = v_{\perp} M_s / q_s B$ and the associated magnetic moment $\mu = M_s v_{\perp}^2 / 2B$ are constant for each species [particles of mass M_s , charge $q_s = Z_s e$ (with e the elementary charge) and perpendicular velocity v_{\perp}], meaning that all particles of a species have the same gyromotion. So do we omit in the following the usual summation over different values of μ for a given species (we refer the reader to Ref. 26 for a water bag analysis of this problem). For each species s , the Vlasov equation then reads:

$$\partial_t f_s + \langle \mathbf{v}_E(\mathbf{r}, t) \rangle_s \cdot \nabla_{\perp} f_s + v_{\parallel} \partial_z f_s + \frac{Z_s}{M_s} \langle E(\mathbf{r}, t) \rangle_s \partial_{v_{\parallel}} f_s = 0. \quad (1)$$

We note here that by using gyroaverage (denoted by $\langle \cdot \rangle_s$) and considering a constant perpendicular velocity associated to gyromotion, only the parallel velocity remains an independent variable.

The quasineutrality equation ensures the coupling between the different ion species and electrons, that are moreover assumed adiabatic with a low electrostatic energy $e\phi \ll T_e$,

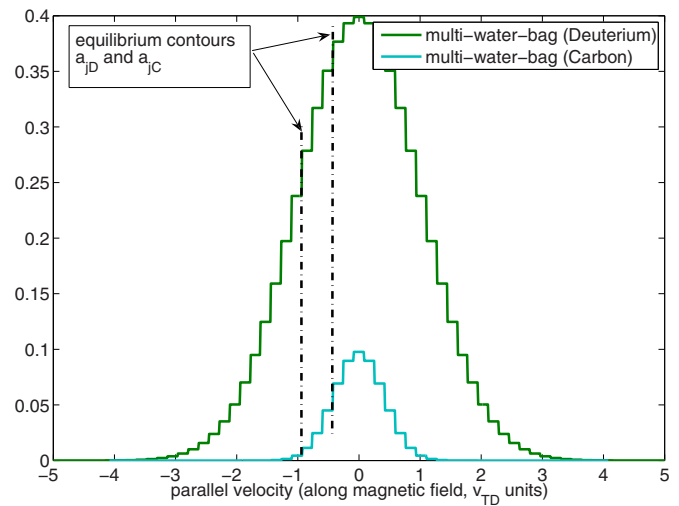


FIG. 1. (Color online) Maxwellian multiwater-bag distribution functions plotted against the parallel velocity direction [case of deuterium (d) and carbon (c), v_{TD} units].

$$n_{e0} \left(1 + \frac{e\phi(\mathbf{r}, t)}{T_e} \right) = \sum_s Z_s \left(\nabla_{\perp} \cdot \left[\frac{M_s n_{s0}}{q_s B^2} \nabla_{\perp} \phi(\mathbf{r}, t) \right] + \int_{-\infty}^{+\infty} \langle f_s(\mathbf{R}, v_{\parallel}, t) \rangle_s dv_{\parallel} \right). \quad (2)$$

ϕ , E , and \mathbf{v}_E are, respectively, electrostatic potential and field, and the corresponding electric drift $\mathbf{v}_E = -\nabla\phi \times \mathbf{B} / B^2$. Each ion species s is defined with its charge $q_s = Z_s e$, mass M_s and equilibrium density n_{s0} . T_e is the electron temperature, e their charge and n_{e0} their equilibrium density. Finite Larmor Radius effects are contained in the gyroaveraged distribution function $\langle f_s(\mathbf{R}, v_{\parallel}, t) \rangle_s$, and in the first term of the left-hand side of the quasi neutrality Eq. (2), commonly known as the polarization effect.

We now represent each species with a water bag distribution function along the velocity parallel to the magnetic field, given by the sum of N_s Heaviside step functions Y ,

$$f_s = \sum_{j=1}^{N_s} A_{sj} \{ Y[v_{\parallel} - v_{sj}^-(\mathbf{R}, t)] - Y[v_{\parallel} - v_{sj}^+(\mathbf{R}, t)] \}. \quad (3)$$

Each bag j is enclosed by positive and negative velocity contours v_{sj}^{\pm} and has an height A_{sj} (Fig. 1), while the total number of bags N_s is free for any species. Moreover and accordingly to the conservation property of phase space measured by the distribution function, the height A_{sj} of each bag is a constant of motion. By inserting multiwater-bag distributions Eq. (3) into Eqs. (1) and (2), we obtain

$$\begin{aligned} \partial_t v_{sj}^{\pm}(\mathbf{R}, t) + \langle \mathbf{v}_E(\mathbf{r}, t) \rangle_s \cdot \nabla_{\perp} v_{sj}^{\pm}(\mathbf{R}, t) + v_{sj}^{\pm}(\mathbf{R}, t) \partial_z v_{sj}^{\pm}(\mathbf{R}, t) \\ = \frac{q_s}{M_s} \langle E(\mathbf{r}, t) \rangle_s, \end{aligned} \quad (4)$$

$$n_{e0} \left(1 + \frac{e\phi(\mathbf{r}, t)}{T_e} \right) = \sum_s Z_s \left\{ \nabla_{\perp} \cdot \left[\frac{M_s n_{s0}}{q_s B^2} \nabla_{\perp} \phi(\mathbf{r}, t) \right] + \sum_{j=1}^{N_s} A_{sj} \langle v_{sj}^+(\mathbf{R}, t) - v_{sj}^-(\mathbf{R}, t) \rangle_s \right\}. \quad (5)$$

We can rewrite these equations by defining for each species a density $n_{sj} = A_{sj}(v_{sj}^+ - v_{sj}^-)$, an average velocity $u_{sj} = (v_{sj}^+ + v_{sj}^-)/2$, and a partial pressure $p_{sj} = M_s n_{sj}^3 / 12 A_{sj}^2$ relatively to each bag,

$$\partial_t n_{sj} + \langle \mathbf{v}_E \rangle_s \nabla_{\perp} n_{sj} + \partial_z u_{sj} n_{sj} = 0, \quad (6)$$

$$\partial_t u_{sj} + \langle \mathbf{v}_E \rangle_s \nabla_{\perp} u_{sj} + u_{sj} \partial_z u_{sj} = \frac{q_s}{M_s} \langle E \rangle_s - \frac{1}{M_s n_{sj}} \partial_z p_{sj}, \quad (7)$$

$$n_{e0} \left[1 + \frac{e\phi}{T_e} \right] = \sum_s Z_s \left\{ \nabla_{\perp} \cdot \left(\frac{M_s n_{s0}}{q_s B^2} \nabla_{\perp} \phi \right) + \sum_{j=1}^{N_s} \langle n_{sj} \rangle_s \right\}. \quad (8)$$

We recover the hydrodynamic formulation of the water bag equations, providing a continuity Eq. (6) and a Euler Eq. (7) equation for each bag with an exact closure given by the partial pressures $p_{sj} = M_s n_{sj}^3 / 12 A_{sj}^2$. Such a formulation is a typical feature of our modeling choice of a water bag distribution function.²²

III. LINEAR ANALYSIS

In the present section, we derive the expression of the dielectric function $\epsilon(\omega)$ of a multispecies plasma, aiming for obtaining a linear stability threshold. We assume an homogeneous equilibrium along the magnetic axis (z direction) and the orthoradial coordinate (θ), without any equilibrium electric potential. Contours are expressed with an even equilibrium $\pm a_{sj}(r)$ and a fluctuating part w_{sj}^{\pm} . Fluctuating quantities are expanded on a Fourier basis for θ and z ,

$$v_{sj}^{\pm} = \pm a_{sj}(r) + w_{sj}^{\pm}(r) e^{i(m\theta + k_{\parallel} z - \omega t)}, \quad (9)$$

$$\phi = 0 + \delta\phi(r) e^{i(m\theta + k_{\parallel} z - \omega t)}, \quad (10)$$

where m is the orthoradial mode number and k_{\parallel} is the parallel wave vector.

For simplicity, we **neglect finite gyroradius effects** by considering for each species $r_{Ls} = 0$, we then obtain the linearized gyrowater-bag equations,

$$(\omega \mp k_{\parallel} a_{sj}) w_{sj}^{\pm} = \left[k_{\parallel} \frac{q_s}{M_s} \mp \frac{m}{rB} d_r a_{sj} \right] \delta\phi, \quad (11)$$

$$\frac{en_{e0}}{T_e} \delta\phi = \sum_s \left[Z_s \sum_{j=1}^{N_s} A_{sj} (w_{sj}^+ - w_{sj}^-) \right]. \quad (12)$$

The gyrowater-bag multispecies dielectric function is obtained by eliminating contour fluctuations (w_{sj}^{\pm}) given by Eq. (11) into quasineutrality Eq. (12),

$$\epsilon(\omega) = 1 - \frac{T_e}{en_{e0}} \sum_s \left[Z_s n_{s0} \frac{q_s}{M_s} \sum_{j=1}^{N_s} \alpha_{sj} \frac{k_{\parallel}^2 - \omega k_{\theta} \kappa_{sj} / \Omega_{cs}}{\omega^2 - k_{\parallel}^2 a_{sj}^2} \right], \quad (13)$$

where we introduce the bag relative density $\alpha_{sj} = 2a_{sj} A_{sj} / n_{s0}$ and the radial derivative for each equilibrium contour $\kappa_{sj} = d_r \ln a_{sj}$. More usual parameters are the poloidal wave vector $k_{\theta} = m/r$ (r being the radial point considered) and the cyclotron frequency $\Omega_{cs} = q_s B / M_s$. Introducing the parameters $Z_s^* = Z_s T_e / T_s$ and $v_{Ts}^2 = T_s / M_s$, the dielectric plasma function can be written,

$$\epsilon(\omega) = 1 - \sum_s \left[Z_s^* \frac{Z_s n_{s0}}{n_{e0}} v_{Ts}^2 \sum_{j=1}^{N_s} \alpha_{sj} \frac{k_{\parallel}^2 - \omega k_{\theta} \kappa_{sj} / \Omega_{cs}}{\omega^2 - k_{\parallel}^2 a_{sj}^2} \right]. \quad (14)$$

The linear stability threshold is defined with $\epsilon(\omega) = 0$ and $d_{\omega} \epsilon(\omega) = 0$ (Ref. 24). By applying these conditions to the dielectric plasma function Eq. (14), we obtain:

$$\sum_s Z_s^* \frac{Z_s n_{s0}}{n_{e0}} v_{Ts}^2 \left[\sum_{j=1}^{N_s} \alpha_{sj} \frac{k_{\parallel}^2 - \omega k_{\theta} \kappa_{sj} / \Omega_{cs}}{\omega^2 - k_{\parallel}^2 a_{sj}^2} \right] = 1, \quad (15)$$

$$\sum_s Z_s^* \frac{Z_s n_{s0}}{n_{e0}} v_{Ts}^2 \sum_{j=1}^{N_s} \alpha_{sj} \frac{(\omega^2 + k_{\parallel}^2 a_{sj}^2) k_{\theta} \kappa_{sj} / \Omega_{cs} - 2\omega k_{\parallel}^2}{(\omega^2 - k_{\parallel}^2 a_{sj}^2)^2} = 0. \quad (16)$$

We can notice that the calculation of such a threshold is a good illustration of the ability of the water bag model, because in the general case of multiple continuous distribution functions, no analytic expression of the threshold can be derived. In our case, the threshold is accessible very simply by using a ω parametrization of previous Eqs. (15) and (16).

IV. LINEAR STABILITY

We will now focus on the case of a **two species plasma** (indexed D for fixed deuterium and s for varying species in the following). In such a two species case, the linear threshold of stability [Eqs. (15) and (16)] is a surface in a space of four dimensions defined by the density (κ_{nD}, κ_{ns}) and temperature (κ_{TD}, κ_{Ts}) gradients of each species. For representation facilities, we assume the same temperature profile for each species. The density gradients are linked with respect to the definition of the effective charge Z_{eff} (introducing its radial derivative $\kappa_{Z_{\text{eff}}}$),

$$Z_{\text{eff}} = \frac{Z_D^2 n_{D0} + Z_s^2 n_{s0}}{Z_D n_{D0} + Z_s n_{s0}}, \quad (17)$$

$$\kappa_{Z_{\text{eff}}} = \frac{Z_D n_{D0} Z_s n_{s0} (Z_D - Z_s) (\kappa_{nD} - \kappa_{ns})}{(Z_D n_{D0} + Z_s n_{s0})^2 (Z_D^2 n_{D0} + Z_s^2 n_{s0})}, \quad (18)$$

and we will consider two different cases.

- The first one is to consider a flat impurity profile, with an arbitrary density profile for the other species. The effective charge profile $\kappa_{Z_{\text{eff}}}$ is then

$$\kappa_{Z_{\text{eff}}} = \frac{Z_D n_{D0} Z_s n_{s0} (Z_D - Z_s)}{(Z_D n_{D0} + Z_s n_{s0})^2 (Z_D^2 n_{D0} + Z_s^2 n_{s0})} \kappa_{nD}. \quad (19)$$

- The second case consists in forcing the impurities in following main ions ($\kappa_{ns} = \xi \kappa_{nD}$), while the effective charge radial profile is given by the definition of $\kappa_{Z_{\text{eff}}}$ Eq. (18).

We apply in the following the results of linear analysis [Eqs. (14)–(16)] to three practical cases of mixed plasmas. The main species is chosen to be deuterium while the other one is detailed below.

- To ensure fusion reactions at low temperature, tritium must be present in a Tokamak. Its properties ($Z_T=1$ et $M_T \approx 3m_p$) are closed to the deuterium reference.
- Carbon ($M_C \approx 12m_p$, $Z_C=6$) often constitutes Tokamak wall elements. It gives an interesting intermediary value of charge and mass values.
- To study the effect of heavy particles the tungsten is chosen ($M_W \approx 184m_p$, $Z_W \approx 40$),²⁷ which is a good candidate for long lifetime ITER divertor and first wall.²⁸

A. Water bag parameters

The water bag model replaces an imaginary pole with a finite number of real resonances that are associated to discontinuities of the water bag distribution function along the velocity coordinate.^{21,29,30} Such discontinuities correspond to values $\omega = \pm k_{\parallel} a_{sj}$, as can be seen in the expression of the dielectric plasma function Eq. (14). As shown in Fig. 1, we superpose discontinuities linked to each species by choosing the same interval between two bags Δa .

Such a superposition allows us to treat easily the real poles of the dielectric plasma function, that can be expressed as a rational function of two polynoms. The roots are degenerate in the velocity interval where the two species are defined.

Practically, regarding the velocity grids relative to each species, we use constant and equal interval lengths, $\Delta a_D = \Delta a_s = \Delta a$. For each species s (including deuterium), the cut-off velocity a_{N_s} is chosen to be equal to five thermal velocities,

$$\forall j \leq N_s, \quad a_{js} = \left(j + \frac{1}{2} \right) \Delta a_s,$$

$$N_s: \quad 5v_{Ts} = \left(N_s + \frac{1}{2} \right) \Delta a_s.$$

The velocity equilibrium contours a_{sj} being fixed, the bag densities α_{sj} as well as the logarithmic gradients of equilibrium velocities κ_{sj} remain to be given. As detailed in a previous paper,³¹ we used a moment sense equivalence with respect to Maxwellian distribution functions

$$f_s = \frac{n_{s0}}{\sqrt{2\pi} v_{Ts}} e^{-v_{\parallel}^2 / v_{Ts}^2}, \quad (20)$$

that allows us to link the unknown water bag parameters α_{sj}, κ_{sj} to the Maxwellian moments.

In the following we will present stability diagrams in the plane of density gradient (κ_{nD}) and temperature gradient (κ_{TD}) of the deuterium. As usual in the study of temperature gradient modes, the unstable areas are the ones containing second or fourth quarters of the stability plane. Such diagrams present a structure relative to our choice of water bag distribution functions. For detailed explanations about the specificity of a water bag representation, we refer the reader to previous articles.^{23,24}

The important information we need to precise is that such water bag stability diagrams present a lobe-like structure, where each lobe is related to a given parallel velocity population. The fastest particles are located near ($\kappa_{nD} = 0$, $\kappa_{TD} = 0$) couples, while the slow ones follow the $\eta \rightarrow 2$ asymptote in the case of a pure plasma (η being the ratio between temperature and density gradients of main ions $\eta = \kappa_{TD} / \kappa_{nD}$).

It is important to notice that these two areas can be associated to fluid (for the η branch) and kinetic parts (region close to zero) of the plasma response.²⁴ By considering the case of a one-bag plasma with one ion species, the ratio between temperature and density gradients is fixed such that η is strictly equal to 2. In that case no instability can develop. On the contrary, the linear stability frontier of a single ion plasma described by a multiwater-bag Maxwellian equilibrium recovers the $\eta=2$ value as an asymptote for the large density and temperature gradients limit.

In the numerical results presented in the following, length are expressed in k_{\parallel} units, velocities are normalized with respect to the deuterium thermal velocity, $\hat{v} = v / v_{TD}$, and frequencies are consequently expressed in k_{\parallel} / v_{TD} units. Since there is no k_{θ} mode selection in the zero Larmor radius approximation, we can take $k_{\theta} r_{LD} = 1$ without a loss of generality.

B. Flat density profile of impurities

By considering a flat density profile, we simplify to dilution effects the impact of impurities on the linear stability threshold. In the case of tritium, we are considering two populations with comparable density values. We plot in Fig. 2(a) the linear stability thresholds of a mixed D-T plasma, for different values of tritium relative density. We choose to use a relatively large bag number ($N_D=30$, $N_C=24$), in order to neglect the water bag typical lobe-like structure.²⁴ We report in Fig. 2(b) the dependence of the linear growth rate (γ in $k_{\parallel} v_{TD}$ units) on the density gradient of main deuterium ions κ_{nD} for a fixed value of temperature gradient κ_T .

The mixed deuterium–tritium plasma exhibits two kinds of response (see upper part of Fig. 2). We can distinguish stabilized areas related to small values of the temperature profile, linked to high velocities classes of particles. But the plasma is more affected in the fluid branch, associated to slow particles, where the tritium effect is to destabilize the plasma. Regarding the linear growth rate (lower part of Fig. 2), we observe quantitatively two antagonist effects: γ decreases around κ_{nD} close to zero (kinetic branch), while the unstable domain increases for higher absolute values of the

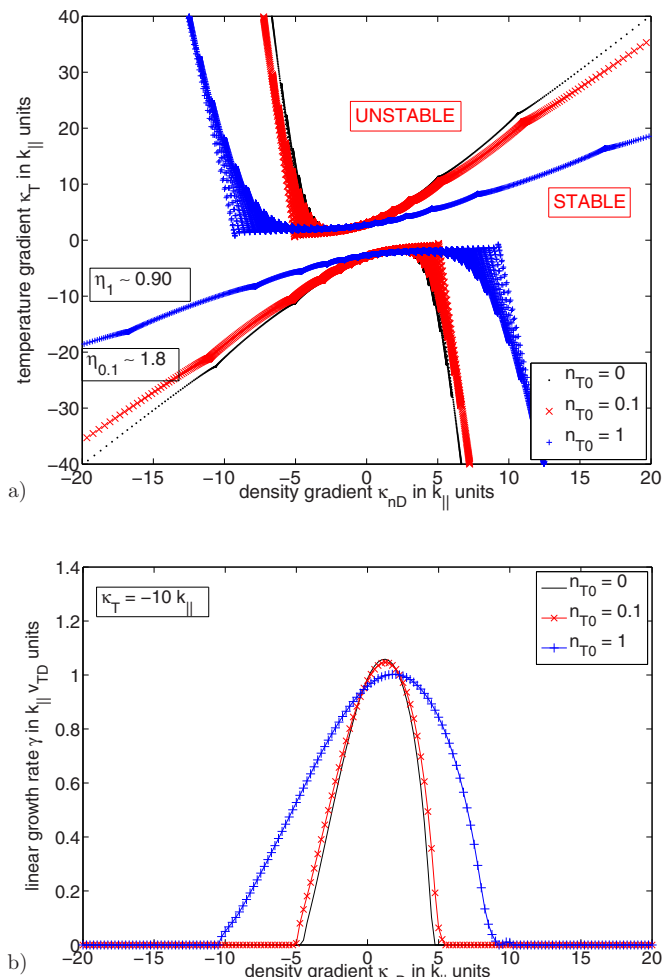


FIG. 2. (Color online) Impact of relative density of impurities on the linear threshold of stability (a) in the plane of deuterium gradients (κ_{nD} , κ_T in k_{\parallel} units), and on the linear growth rate γ (b) along the density gradient κ_{nD} for a given value of the temperature gradient $\kappa_T = -10k_{\parallel}$. Case of a deuterium–tritium plasma ($N_D=30$, $N_T=24$, $a_{\max D}=5v_{TD}$, $a_{\max T}=4.08v_{TD}$, $\kappa_{nT}=0$).

density gradient (fluid branch). These effects become perceptible from values of the relative tritium density equal to 10% of the main deuterium density.

Next, we represent in Fig. 3 the linear stability threshold (a) and the associated linear growth rate (b) of a plasma with deuterium and a relatively high population of carbon ions (10% of the deuterium density, $Z_{\text{eff}}=2.875$). Effects ever observed in the case of deuterium–tritium plasma are recovered. The linearly unstable area is extended by adding carbon to the deuterium plasma, proportionally to the relative carbon density ($n_{C0}=0.1n_{D0}$ shows a stability diagram comparable to $n_{T0}=N_{D0}$).

Moreover the more unstable values of the linear growth rate located around flat deuterium density profile, are decreased by more than 20%. That is very high when compared to the case of tritium impurities (even with $n_{T0}=n_{D0}$) that showed very similar values of growth rates.

Tungsten exhibits very high values of charge and mass. To describe its effect on the linear stability threshold of a deuterium plasma, we choose to deal with a very high num-

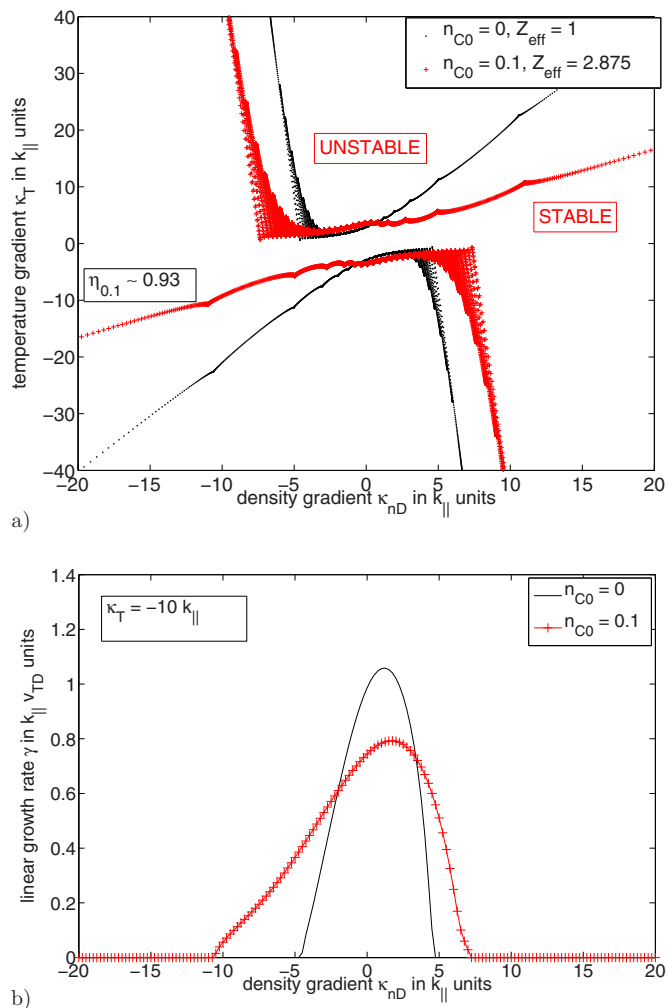


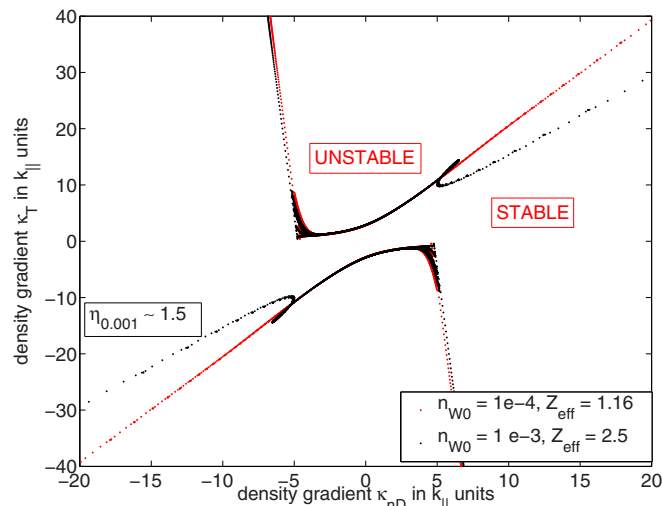
FIG. 3. (Color online) Impact of relative density of impurities on the linear threshold of stability (a) in the plane of deuterium gradients (κ_n , κ_T), and on the linear growth rate γ (b) along the density gradient κ_{nD} for a given value of the temperature gradient $\kappa_T = -10k_{\parallel}$. Case of a deuterium–carbon plasma ($N_D=30$, $N_C=12$, $a_{\max D}=5v_{TD}$, $a_{\max C}=2.04v_{TD}$, $\kappa_{nC}=0$).

ber of bags in order to have a satisfying description of the tungsten equilibrium distribution function, according to the large mass ratio ($N_D=500$, $N_W=52$).

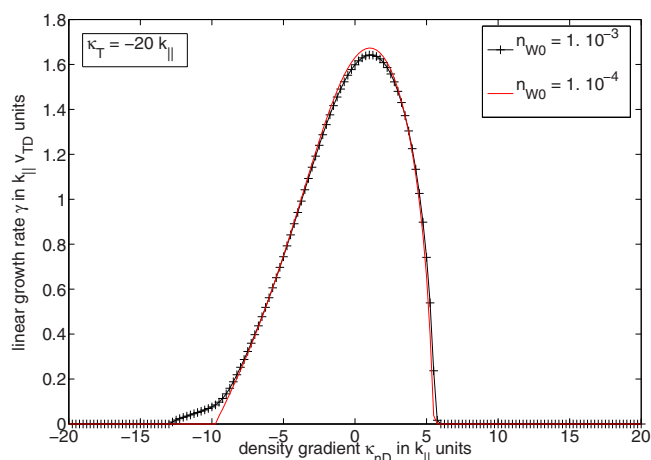
We draw in Fig. 4 the linear stability threshold (a) and the linear growth rate (b) of a deuterium–tungsten plasma. A typical effect is that the addition of tungsten gives rise to a secondary lobe-like structure, distinct from the deuterium relevant one. Such a separation is due to the fact that the distribution function of the tungsten population is very different from the deuterium one, especially the thermal velocities.

In the lower part of Fig. 4, we use a constant temperature gradient $\kappa_T = -20k_{\parallel}$. That value is assumed different from previous cases (Figs. 3 and 2) in order to be in the second lobe relative to the tungsten ions. We observe that the growth rate related to the second lobe takes very low values (less than 10% of the maximum value), while the maximum of growth rate very slowly decreases around $\kappa_{nD}=0$ values.

Whatever the species we consider, we obtain two different responses of the plasma, depending on the values of density and temperature profiles.



a)



b)

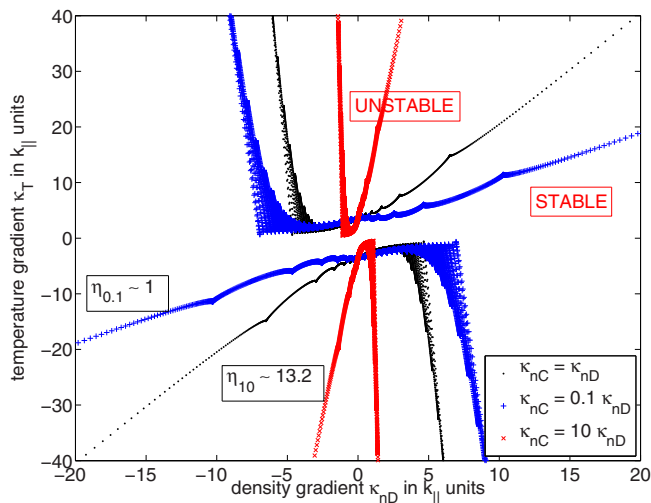
FIG. 4. (Color online) Impact of relative density of impurities on the linear threshold of stability (a) in the plane of deuterium gradients (κ_n, κ_T) and on the linear growth rate γ (b) along the density gradient κ_{nD} for a given value of the temperature gradient $\kappa_T = -20k_{||}$. Case of a deuterium-tungsten plasma ($N_D=500, N_W=52, a_{maxD}=5v_{TD}, a_{maxW}=0.52v_{TD}, \kappa_{nW}=0$).

- The first one, very low, is a stabilization for small values of density gradients (kinetic branch).
- The second effect is an important destabilization of the mixed plasma, in regions with high values of temperature and density profiles (fluid branch).

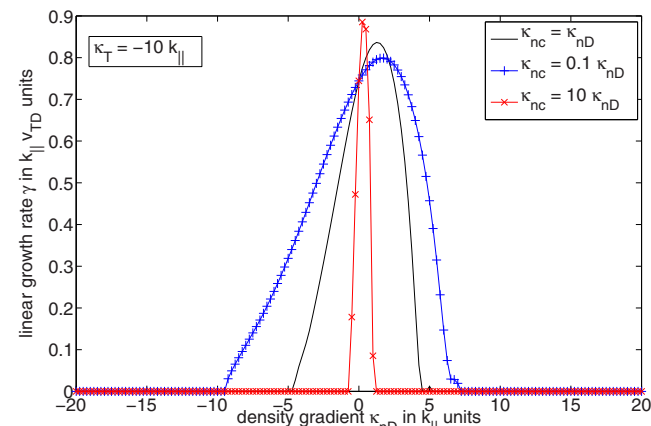
These two effects are in agreement with Ref. 12, where authors used the assumption of a flat effective charge profile. The increase of impurity relative ratio, and/or their charge and mass leads to a stabilizing effect in the flat density limit ($\kappa_{nD}, \kappa_{TD} \approx 0.0$ in our stability diagrams). On the other hand, the low frequency branch, corresponding to the fluid branch presents a destabilization of the plasma that is proportional to the relative density and/or charge and mass of impurities. Such a result has been observed by other authors.¹⁴

C. Effect of density gradient of impurities

We focus here on the case of a plasma composed of deuterium and carbon. We study the effect of the radial profile of impurities on the linear stability of the plasma in the



a)



b)

FIG. 5. (Color online) Impact of density peaking of impurities on the linear threshold of stability (a) in the plane of deuterium gradients (κ_n, κ_T), and on the linear growth rate γ (b) along the density gradient κ_{nD} for a given value of the temperature gradient $\kappa_T = -10k_{||}$. Case of a deuterium-carbon plasma ($N_D=30, N_C=12, a_{maxD}=5v_{TD}, a_{maxC}=2.04v_{TD}, n_{C0}=0.1, \text{ and } Z_{eff}=2.9$).

plane of the main ions parameters (κ_{nD} and κ_{TD}). The temperature profiles are equaled ($\kappa_{TC} = \kappa_{TD}$), and we connect the density gradients in any point of the stability diagram with a fixed coefficient

$$\kappa_{nC} = \xi \kappa_{nD}. \tag{21}$$

Under such a condition, the effective charge profile Eq. (18), is easily linked to the density gradient of deuterium ions

$$\kappa_{Z_{eff}} = \frac{Z_D n_{D0} Z_C n_{C0} (Z_D - Z_C) (1 - \xi) \kappa_{nD}}{(Z_D n_{D0} + Z_C n_{C0})^2 (Z_D^2 n_{D0} + Z_C^2 n_{C0})}. \tag{22}$$

We represent in Fig. 5 the linear stability diagram of a plasma mixing deuterium and carbon. The ratio between the density of deuterium and the density of carbon is constant. We choose a relatively high value $n_{C0} = 0.1 n_{D0}$, in order to enlight the effect of the carbon density peaking.

We observe that the stability threshold strongly depends on the ratio between radial density gradients of deuterium and carbon. In the case of a carbon density gradient lower than the deuterium one (blue curve, $\kappa_{nC} = 0.1 \kappa_{nD}$), the fluid

asymptote ($\eta_{0,1} \sim 1$) corresponding to large values of density and temperature gradients is lower than the classical value ($\eta=2$), and the unstable area globally increases.

On the contrary, if we consider an impurity profile more peaked than the majority ions (red curve, $\kappa_{nC}=10\kappa_{nD}$), we observe an exactly opposite effect. The unstable area is much less extended, and the asymptotic value of the η ratio is clearly greater than the usual value ($\eta_{10} \sim 13.2$).

Representing the linear growth rate in Fig. 5(b) enlightens these facts: the density peaking of impurity decreases the width of the unstable area, while it increases its maximum value. In other terms, the density peaking of the impurities stabilizes the slowly moving particles of the plasma associated to the fluid description, and destabilizes the fast ones. Such results are in qualitative agreement with older works.^{12,14}

V. DISCUSSION

Linear stability of a multispecies plasma has been discussed within the framework of a cylindrical plasma column (i.e., without magnetic curvature and/or magnetic gradient effect). An interesting feature of the water bag linear analysis is that there is no ambiguity about the linear growth rates, because the water bag dielectric function presents at the most a unique couple of complex conjugate roots.

The stability threshold has been shown to depend on the relative densities of species. The coupling induced by the impurities can destabilize the plasma. The amplitude of destabilization is proportional to the mass of impurity considered. In the case of a flat density profile of impurities, increasing relative density of heavy ions destabilizes the plasma in the fluid branch, while it stabilizes the plasma in the central area associated to small density gradients (kinetic branch).

If the density profile is not flat, we have chosen to link it to the main ions density profile by using a linear relation. The relative peaking of impurities can stabilize (in the case of impurities more peaked than the main ions) or destabilize (with impurities more flat than main ions) the fluid branch of the Ion Temperature Gradient (ITG) linear stability diagram. The two antagonist effects shown with flat density by playing on the density ratios are recovered: the peaking of impurity density profile plays a role comparable to the increase of their relative density or mass.

The next step for the gyrowater bag model is its extension to toroidal geometry, that is currently under investigation.³² Another interesting feature would be to take into account kinetic electrons with a water bag model, the main difficulty would be the large discrepancy in thermal

velocities due to the ion to electron mass ratio. But such a difficulty is not due to our particular choice of a water bag representation.

- ¹T. Pierre, G. Leclert, and F. Braun, *Rev. Sci. Instrum.* **58**, 6 (1987).
- ²O. Grulke, T. Klinger, and A. Piel, *Phys. Plasmas* **6**, 788 (1999).
- ³C. Schröder, O. Grulke, T. Klinger, and V. Naulin, *Phys. Plasmas* **11**, 4249 (2004).
- ⁴E. Wallace, E. Thomas, A. Eadon, and J. Jackson, *Rev. Sci. Instrum.* **75**, 5160 (2004).
- ⁵R. G. Greaves, J. Chen, and A. K. Sen, *Plasma Phys. Controlled Fusion* **34**, 1253 (1992).
- ⁶T. Fülöp and J. Weiland, *Phys. Plasmas* **13**, 112504 (2006).
- ⁷N. Dubuit, X. Garbet, T. Parisot, R. Guirlet, and C. Bourdelle, *Phys. Plasmas* **14**, 042301 (2007).
- ⁸D. R. Ernst, P. T. Bonoli, P. J. Catto, W. Dorland, C. L. Fiore, R. S. Granetz, M. Greenwald, A. E. Hubbard, M. Porkolab, M. H. Redi, J. E. Rice, K. Zhurovich, and Alcator C-Mod Group, *Phys. Plasmas* **11**, 2637 (2004).
- ⁹C. Estrada-Mila, J. Candy, and R. E. Waltz, *Phys. Plasmas* **12**, 022305 (2005).
- ¹⁰A. Casati, C. Bourdelle, X. Garbet, and F. Imbeaux, *Phys. Plasmas* **15**, 042310 (2008).
- ¹¹C. Angioni, A. G. Peeters, G. V. Pereverzev, A. Bottino, J. Candy, R. Dux, E. Fable, T. Hein, and R. E. Waltz, *Nucl. Fusion* **49**, 055013 (2009).
- ¹²R. Paccagnella, F. Romanelli, and S. Briguglio, *Nucl. Fusion* **30**, 545 (1990).
- ¹³M. Fröjdth, H. Nordman, and J. Weiland, *Phys. Scr.* **43**, 186 (1991).
- ¹⁴M. Fröjdth, M. Lijleström, and H. Nordman, *Nucl. Fusion* **32**, 419 (1992).
- ¹⁵C. Bourdelle, X. Garbet, F. Imbeaux, A. Casati, N. Dubuit, R. Guirlet, and T. Parisot, *Phys. Plasmas* **14**, 112501 (2007).
- ¹⁶G. M. Staebler, J. E. Kinsey, and R. E. Waltz, *Phys. Plasmas* **14**, 055909 (2007).
- ¹⁷D. C. DePackh, *J. Electron. Control* **13**, 417 (1962).
- ¹⁸F. Hohl, *Phys. Fluids* **12**, 230 (1969).
- ¹⁹M. R. Feix, F. Hohl, and L. D. Staton, in *Nonlinear Effects in Plasmas*, edited by G. Kalman and M. R. Feix (Gordon and Breach, New York, 1969), pp. 3–21.
- ²⁰H. L. Berk and K. V. Roberts, in *Methods in Computational Physics*, edited by B. Alder, S. Fernbach and M. Rotenberg (Academic, New York, 1970), Vol. 9, p. 29.
- ²¹P. Bertrand, M. Gros, and G. Baumann, *Phys. Fluids* **19**, 1183 (1976).
- ²²M. Gros, P. Bertrand, and M. R. Feix, *Plasma Phys.* **20**, 1075 (1978).
- ²³N. Besse, P. Bertrand, P. Morel, and E. Gravier, *Phys. Rev. E* **77**, 056410 (2008).
- ²⁴P. Morel, E. Gravier, N. Besse, R. Klein, A. Ghizzo, P. Bertrand, X. Garbet, P. Ghendrih, V. Grandgirard, and Y. Sarazin, *Phys. Plasmas* **14**, 112109 (2007).
- ²⁵E. Gravier, R. Klein, P. Morel, N. Besse, and P. Bertrand, *Phys. Plasmas* **15**, 122103 (2008).
- ²⁶R. Klein, E. Gravier, P. Morel, N. Besse, and P. Bertrand, *Phys. Plasmas* **16**, 082106 (2009).
- ²⁷R. Neu, K. B. Fournier, D. Schlögl, and J. Rice, *J. Phys. B* **30**, 5057 (1997).
- ²⁸O. Gruber, A. C. C. Sips, R. Dux, T. Eich, J. C. Fuchs, A. Herrmann, A. Kallenbach, C. F. Maggi, R. Neu, T. Pütterich, J. Schweinzer, J. Stober, and ASDEX Upgrade Team, *Nucl. Fusion* **49**, 115014 (2009).
- ²⁹N. G. Van Kampen, *Physica* **21**, 959 (1955).
- ³⁰K. M. Case, *Ann. Phys. (N.Y.)* **7**, 349 (1959).
- ³¹P. Morel, E. Gravier, N. Besse, and P. Bertrand, *Commun. Nonlinear Sci. Numer. Simul.* **13**, 11 (2008).
- ³²R. Klein, Ph.D. thesis, Université Henri Poincaré Nancy, 2009.